

1 **Electronic supplementary information (ESI)**

2

3 Huaizhi Yang,^a Yuqi Wan,^a Qingrong Cheng,^{*a}, Hong Zhou,^a Zhiquan Pan,^a Yan Liu.^b

4 ^a School of Chemistry and Environmental Engineering, Wuhan Institute of Technology, Wuhan,
5 430205, PR China.

6 ^b Shenzhen Puhua System Technology Co., Ltd, Shenzhen, 518129, PR China.

7

8 Corresponding authors:

9 *(Q.C.) E-mail: chengqr383121@sina.com

10

11

12

13

14

15

16

17

18

19

20

21

22

23

24

25

26

Total number of pages: 9

27

Total number of Tables: 2

28

Total number of Figures: 6

29

31 **The characterization methods and evaluation of** 32 **photocatalytic performance**

33 Transmission electron microscopy (TEM, FEI TALOS F200) was used to characterize the internal
34 and microstructural information of the samples (HRTEM measures the lattice information of
35 substances), and the basic element composition distribution (EDX) was obtained by equipped with
36 an energy dispersive X-ray spectrometer. Ultraviolet-Visible (UV-Vis) diffuse reflectance
37 spectroscopy (DRS) was measured using a West Wisteria UV-2600 spectrometer with barium
38 sulfate as a reference. X-ray photoelectron spectroscopy (XPS) was performed using the 250Xi-
39 XPS photoelectron spectrometer of the thermal calibration laboratory and aluminum $K\alpha$ ray
40 resources. The change in binding energy was taken as the internal standard at the C1s level at
41 284.8 eV. The patterns collected on a BrukerD8 advanced X-ray diffractometer (XRD) were used
42 to analyze the surface phase composition of the materials, scans over a test angle range of 5° to
43 90° at a rate of 5° min^{-1} . ESR measured by German Bruker (A300), it is used to detect the content
44 of active species in the process of photoreaction.

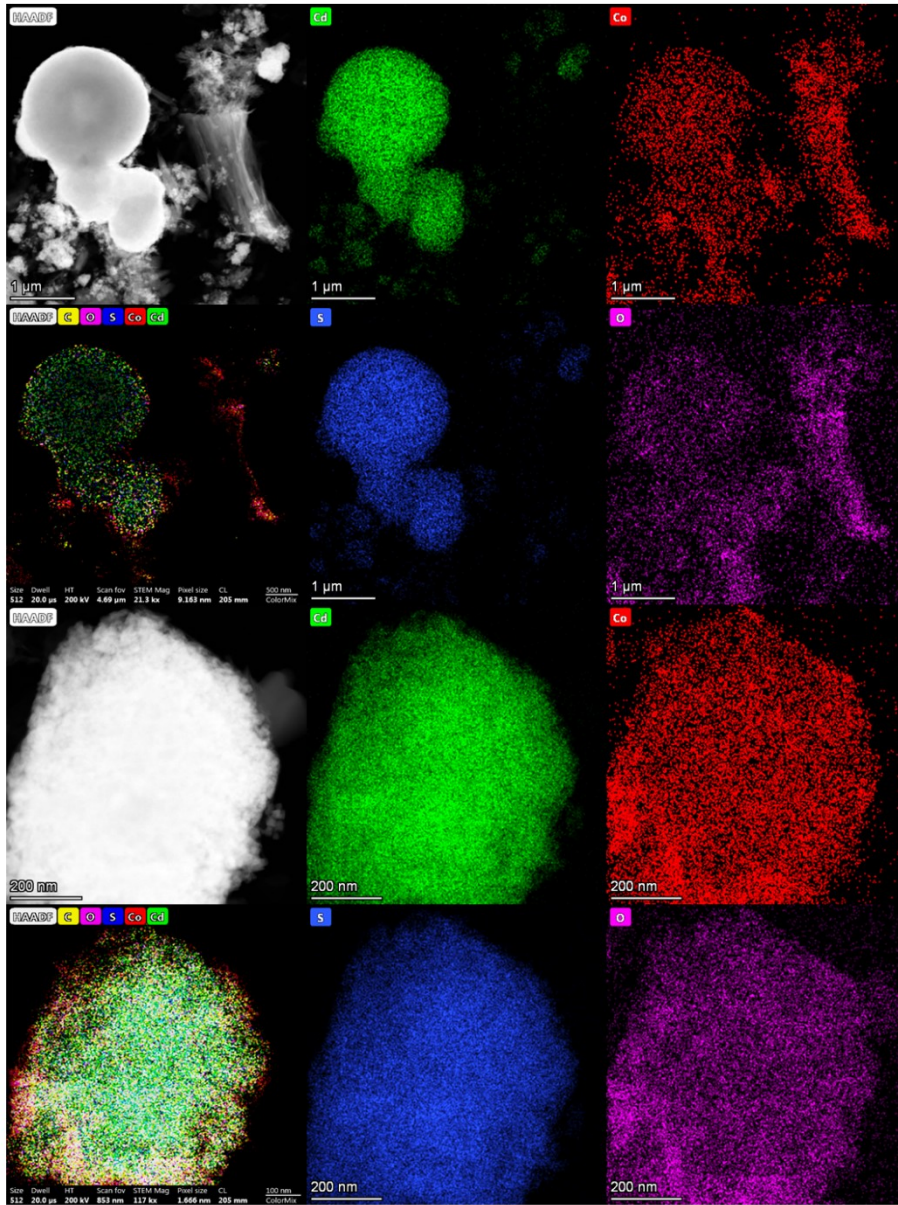
45 Electrochemical measurements were carried out on an electrochemical workstation (CHI760E
46 instruments) connected to a standard three-electrode system, namely the working electrode
47 prepared from the test sample, a platinum plate as the counter electrode, and a saturated Ag/AgCl
48 as the reference electrode. The working electrode was prepared as follows: Weigh 10mg of the
49 sample and pour it into a 5 mL EP tube, added 2 mL Nafion injection solution (Nafion:
50 isopropanol = 1:25), and sonicated for 15 min. Each time, 10 microliters were dropped onto the
51 conductive glass surface with a micro-injector, dispersed evenly, dried under a sun lamp, and the
52 operation was repeated 3 times. The test solution was 0.5 M sodium sulfate aqueous solution.
53 Electrochemical impedance spectroscopy (EIS) data were measured directly at the electrochemical
54 workstation, the frequency range of the circuit potential was 1 Hz to 100 kHz, and the test voltage
55 was 1.5 eV. The EIS was fitted by ZView2 software. Transient Photocurrent Response (PC) of the
56 sample was carried out under sun light conditions (300 W xenon lamp), with the light on for 30 s
57 and the light off for 30 s as a cycle, for 6 consecutive cycles. Mott-Schottky's measurement
58 experiments were performed at frequencies at 500 Hz and 1000 Hz, and the potential changed

59 from -2.0 to 1.5 eV.

60 Photocatalysis experiments included organic pollutant degradation experiments and hydrogen
61 production experiments. The ability of photocatalysts to degrade organic pollutants can be judged
62 by measuring the changes in the absorbance (positions of characteristic peaks) of organics under
63 visible light irradiation. The light source was visible light (with a 420 nm filter). First, 50 mL of
64 30 mg/L TC solution was poured, 3 mL of the solution was taken out, and the measured
65 absorbance was recorded as the initial absorbance (C_{-30}). Then, 10 mg of the photocatalyst was
66 added, and the catalyst was magnetically stirred for 30 min in the dark to reach the adsorption-
67 desorption equilibrium. After the light-proof treatment, 3 mL of the solution was taken out, and the
68 measured absorbance was recorded as the absorbance at 0 min of illumination (C_0). During the
69 photoreaction, 3 mL samples were withdrawn from the reactor every 10 min (It is represented by
70 C_t , and it is denoted as C_{10} and C_{20} in turn.). All samples were filtered photocatalysts using
71 organic filters (0.22 μm . organic). The absorption intensity at the maximum wavelength of 357 nm
72 was measured with a UV-Vis spectrophotometer, and the concentration change was reflected by
73 the change of absorbance to evaluate the degradation efficiency. In the photocatalytic degradation
74 cycle experiments, the products were collected by a common centrifugation method. Considering
75 the mass loss, the amount of catalyst added was changed to 20 mg. In each cycle, we only
76 collected samples before dark (C_{-30}), after dark (C_0), and after 60 min of light (C_{60}). At the end of
77 a cycle, the catalyst in the remaining liquid was collected by centrifugation and washed with
78 methanol and after vacuum drying, and then enter a new round of photocatalytic degradation test
79 with a new tetracycline solution. A total of four cycles were carried out to test the stability of the
80 prepared composite photocatalyst. The photocatalytic hydrogen production experiments were
81 carried out in a 150 mL cylindrical quartz reactor with an irradiation area of 28.12 cm^2 and a 300
82 W xenon lamp as the light source (PerfectLight, Labsolar-IIIAG Photocatalytic system). Mixed 30
83 mg of photocatalyst, 80 mL of distilled water, and the prepared sacrificial agent (10 mL of 0.35 M
84 sodium sulfite solution, 10 mL of 0.25 M sodium sulfide solution) evenly, and replaced the air in
85 the container with nitrogen before the reaction, turned on stirring and kept the catalyst suspend in
86 the reaction system, used a syringe needle draws 300 μL of gas per hour from the reactor, and the
87 H_2 generation rate was calculated by gas chromatography (Timei GC7900, TCD, N_2 as carrier).
88 The operation of the photocatalyst cycle test was as follows: after the first hydrogen production

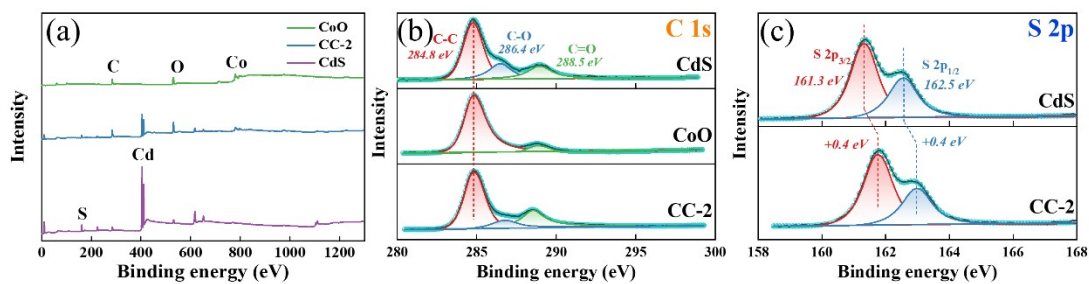
89 experiment, the photocatalyst was collected by centrifugation, washed three times with ethanol,
90 the obtained solid was dried, and transferred to a new solution system, filled with nitrogen again,
91 and carried out for the next hydrogen production experiment, the entire process was repeated four
92 times.

93 The Cambridge Series Total Energy Package (CASTEP) module of Materials Studio program was
94 used to all the DFT calculations. It was calculated using the function GGA-PBE(general gradient
95 approximation- Perdew-Burke-Ernzerhof) and the hybrid functional HSE06 (Heyd-Scuseria-
96 Ernzerhof). Herein, the geometry optimization conditions for CdS and CoO were as follows, the
97 cutoff energies were set to 500 eV and 750 eV, respectively, and the k-points were set to $8 \times 8 \times 5$
98 and $9 \times 9 \times 9$, respectively. The convergence tolerance parameter for the max step size was 0.001 Å,
99 the maximum force was 0.01 eV/Å, the energy change was 1.0×10^{-6} eV/atom, and the maximum
100 stress was 0.02 GPa. For surface structure calculations and heterogeneous junction structure
101 calculations, the interface between CdS and CoO by taking the supercell of 3×3 CdS
102 ($12.60 \text{ \AA} \times 12.60 \text{ \AA}$) and 4×4 CoO ($12.69 \text{ \AA} \times 12.69 \text{ \AA}$), k-points were taken as $2 \times 2 \times 1$, a vacuum layer
103 of 15 Å was constructed to eliminate interactions between periodic structures of surface models,
104 and all the above calculations had been tested for convergence.



105
 106
 107
 108
 109

Figure S1. EDX mapping of the composite photocatalyst.



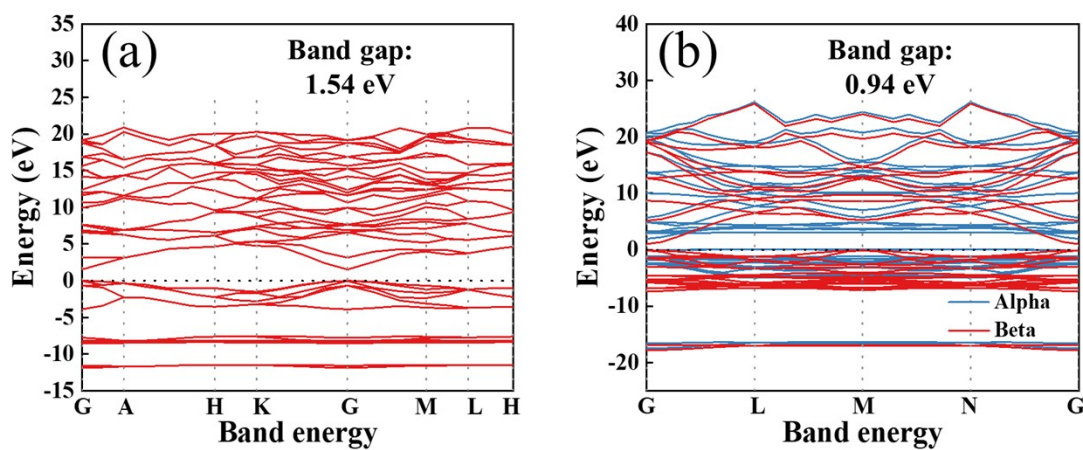
110

111 Figure S2. (a) XPS survey spectra of CdS, CoO and CC-2, (b) C 1s fine spectra of CdS, CoO and CC-2, (c) S

112

2p fine spectra of CdS, and CC-2.

113



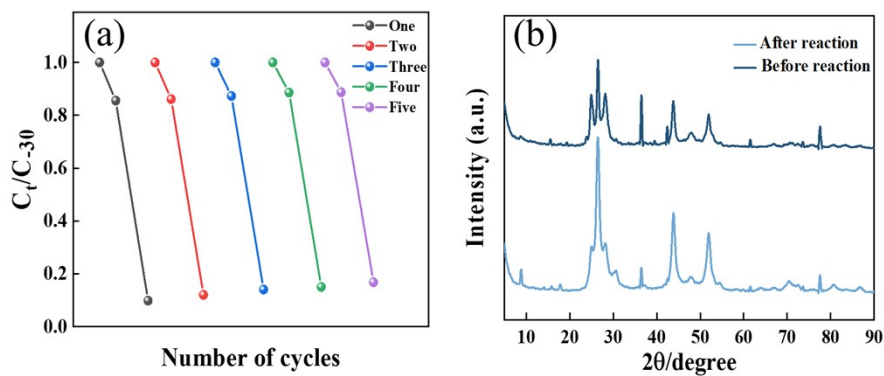
114

115

116 Figure S3. The band energy a of the (a) CdS and (b) CoO, calculated with GGA-PBE.

117

118

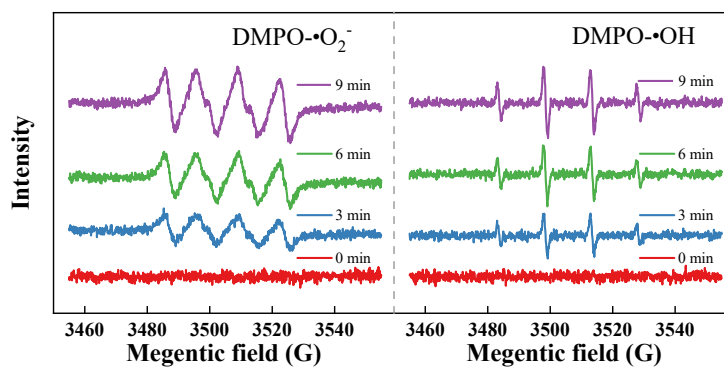


119

120 Figure S4 (a) Degradation efficiency of CC-2 in five cycles, (b) XRD patterns of CC-2

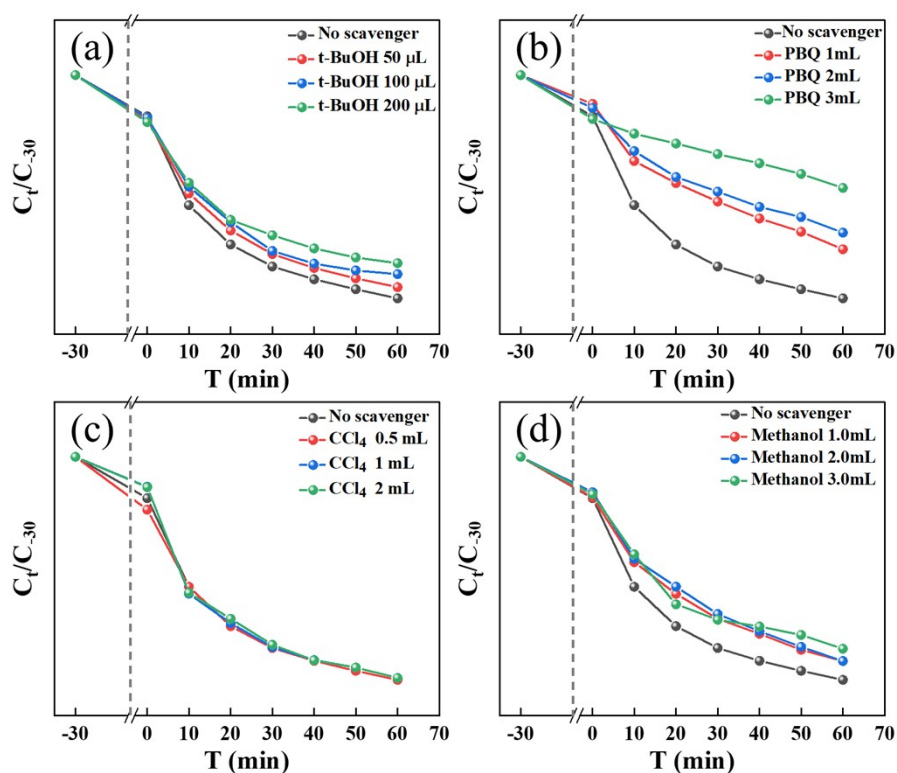
121

before and after cycling.



122
123
124
125

Fig.S5 The ESR spectrum of CC-2 for DMPO- \cdot OH and DMPO- \cdot O₂⁻.



126
127
128

Fig.S6 (a-d) The radical trapping test for the CC-2.

129 **Table S1** Comparison of TC degradation over CC-2 and other

130 photocatalysts.

<i>Catalyst / mg</i>	<i>V (mL) / C₋₃₀ (mg·L⁻¹)</i>	<i>Light source</i>	<i>Time (min)</i>	<i>Result (%)</i>	<i>TOF</i>	<i>Ref</i>
CC-2(CdS/CoO)/10	50/30	Visible light	60	90%	2.25	This work

CDs-CoO/50	100/10	Visible light	60	87%	0.29	[1]
CdS/Ti ₃₂ -oxo-cluster composites /10	50/50	Visible light	60	96.3%	4.01	[2]
CdS/Bi ₄ O ₅ Br ₂ /10	40/20	Visible light	60	85%	1.13	[3]
g-C ₃ N ₄ /CdS/25	50/50	simulated solar light	60	69.63%	1.16	[4]

131 TOF is calculated according to an equation:

$$132 \quad TOF = \frac{C_{-30} \times V_{TC} \times \text{Degradation rate}}{m_{\text{catalyst}} \times t}$$

133

134

135

136 **Table S2** Comparison of the photocatalytic H₂ evolution rates over CC-2 and other
137 photocatalysts.

<i>Photocatalysts</i>	<i>Irrigation</i>	<i>Sacrificial agents</i>	<i>Activity $\mu\text{mol}\cdot\text{g}^{-1}\text{h}^{-1}$</i>	<i>Ref</i>
CC-2(CdS/CoO)	Sun light	Na ₂ SO ₃ and Na ₂ S	4463.5	This work
ZnS/CoO	Visible light	Na ₂ SO ₃ and Na ₂ S	1763.17	[5]
CdS@Ti ₃ C ₂ @CoO	Visible light	nothing	134.46	[6]
CdS/MoS ₂	Visible light		13129	[7]
CdS/Ni-MOF	Visible light	lactic acid	2508	[8]

138

139

140

141 **References:**

142 [1] W. Shi, F. Guo, H. Wang, M. Han, H. Li, S. Yuan, H. Huang, Y. Liu, Z. Kang, Carbon dots
143 decorated the exposing high-reactive (111) facets CoO octahedrons with enhanced photocatalytic
144 activity and stability for tetracycline degradation under visible light irradiation, Appl. Catal., B.
145 219 (2017) 36-44.

146 [2] Q. Zhu, Y. Sun, F. Na, J. Wei, S. Xu, Y. Li, F. Guo, Fabrication of CdS/titanium-oxo-cluster
147 nanocomposites based on a Ti₃C₂ framework with enhanced photocatalytic activity for tetracycline
148 hydrochloride degradation under visible light, *Appl. Catal., B*. 254 (2019) 541-550.

149 [3] W. Cao, C. Jiang, C. Chen, H. Zhou, Y. Wang, A novel Z-scheme CdS/Bi₄O₅Br₂
150 heterostructure with mechanism analysis: Enhanced photocatalytic performance, *J. Alloys Compd.*
151 861 (2021) 158554.

152 [4] G. Li, B. Wang, J. Zhang, R. Wang, H. Liu, Rational construction of a direct Z-scheme g-
153 C₃N₄/CdS photocatalyst with enhanced visible light photocatalytic activity and degradation of
154 erythromycin and tetracycline, *Appl. Surf. Sci.* 478 (2019) 1056-1064.

155 [5] Q. Zhu, S. Xu, Y. Qin, J.C.-H. Lam, Y. Li, Multication and Structure Regulation: Utilizing
156 X - Doped (X = Co, Mn, Cu) ZnS/CoO Hollow Composites to Spatially Propel the Charge for
157 Superior Solar Hydrogen Evolution, *Solar RRL* 7(2) (2022) 2200918.

158 [6] K.Z. Zizheng Ai, Bin Chang, Yongliang Shao, Lei Zhang, Yongzhong Wu, Xiaopeng Hao,
159 Construction of CdS@Ti₃C₂@CoO hierarchical tandem p-n heterojunction for boosting
160 photocatalytic hydrogen production in pure water, *Chem. Eng. J.* (2019) 123130.

161 [7] K. Zhuge, Z. Chen, Y. Yang, J. Wang, Y. Shi, Z. Li, In-situ photodeposition of MoS₂ onto
162 CdS quantum dots for efficient photocatalytic H₂ evolution, *Appl. Surf. Sci.* 539 (2021) 148234.

163 [8] J. Guo, Y. Liang, L. Liu, J. Hu, H. Wang, W. An, W. Cui, Noble-metal-free CdS/Ni-MOF
164 composites with highly efficient charge separation for photocatalytic H₂ evolution, *Appl. Surf. Sci.*
165 522 (2020) 146356.

166

167

168